Disproportional distribution of radioactive elements in the marine ecosystems surrounding the accident site of the Fukushima Daiichi Nuclear Power Plant

Shigeharu Moriya[1, 3, *], Hideaki Otsu[2], Kumiko Kihara[1, 4], Yukari Kato[1], Misao Itouga[1], Kenji Sakata[1], Jun Kikuchi[1, 3], Hiroshi Yamakawa[5, 6] and Jiro Suga[6]

1) RIKEN Center for Sustainable Resource Science, 1-7-22 Suehiro-cho, Tsurumi-ku, Yokohama city, Kanagawa, 230-0045, JAPAN

Shigeharu Moriya, Kumiko Kihara, Yukari Kato, Misao Itouga, Kenji Sakata and Jun Kikuchi

2) RIKEN Nishina Center for Accelerator-Based Science, 2-1 Hirosamwa, Wako city, Saitama, 351-0198, JAPAN

Hideaki Otsu

3) Graduate School of Medical Life Science, Yokohama-city University, 1-7-29 Suehiro-cho, Tsurumi-ku, Yokohama city, Kanagawa, 230-0045, JAPAN

Shigeharu Moriya and Jun Kikuchi

4) Department of Biological and Chemical Systems Engineering, National Institute of Technology, Kumamoto College, 2627 Hirayama-Shinmachi, Yatsushiro-shi, Kumamoto 866-8501, JAPAN

Kumiko Kihara

5) Tokyo University of Marine Science and Technology, 4-5-7 Konan, Minato-ku, Tokyo, 108-8477, JAPAN

Hiroshi Yamakawa

6) Japan Academy of Underwater Sciences, 3-9-1-301 Botan, Koto-ku, Tokyo, 135-0046, JAPAN

Hiroshi Yamakawa and Jiro Suga

*) Corresponding author: Shigeharu Moriya

RIKEN Center for Sustainable Resource Science, 1-7-22 Suehiro-cho, Tsurumi-ku, Yokohama city, Kanagawa, 230-0045, JAPAN

Tel +81-45-508-7221, Fax +81-45-508-7363

smoriya@riken.jp

33 Abstract

34 Background

35 After the Fukushima Daiichi Nuclear Power Plant accident, various surveys were performed
36 to measure the extent of radioactive material contamination in the marine sediments,
37 surface waters, plankton and fish. Six months after the event, relatively high radiocesium
38 contamination could still be detected in the fish and sediment of the coastal demersal
39 environment. To determine the distribution of radioactive material in the demersal
40 ecosystem adjacent to the event, we sampled and analyzed the dominant macroorganisms
41 attached to the seafloor as well as environmental material, including biofilms, from the
42 coastal demersal environment around Hisanohama Port, which is less than 30 km south of
43 the accident site.

44

45 Results

46 Our results showed that variable ratios of radiosilver/radiocesium occurred in the
47 macrobenthos, macroalgae and sediment samples. However, the biofilm samples displayed
48 high radiocesium contamination but did not show radiosilver contamination.

49

50 Conclusions

51 These findings suggest that several different entry paths are available for radioactive

52 elements to access the biological components of the ecosystem, and these paths may explain

53 the disproportional and patchy distribution of radioactive elements among marine

54 ecosystems.

55

56 Keywords

57 Radio isotope, Marine eco-system, Biofilm

58

59 Background

60 Following the Great East Japan Earthquake and catastrophic tsunami in March of 2011,

61 the Fukushima Daiichi Nuclear Power Plant (FDNPP) accident led to the release of large

62 amounts of radioactive materials into the atmosphere and marine environment.

63 This environmental input of radioactive elements from the FDNPP introduced into the

64 marine waters a variety of radioisotopes, especially radiocesium isotopes. Public monitoring

65 showed that during the several months after the first explosion at the FDNPP, a rapid
66 decrease in radioisotopes was observed in the nearby seawater. A joint official survey team
67 from the Tokyo Power Electric Company (TEPCO), Fukushima prefectural government and
68 the Japanese Ministry of Education, Culture, Sports, Science and Technology (MEXT)
69 reported that the ^{137}Cs contamination level in the seawater quickly decreased from over 10 k
70 Bq/liter to less than 100 Bq/liter within a 2-month period, whereas the ^{137}Cs found in the
71 ocean sediments was continuously observed over this period at levels between 100 Bq/dry kg
72 and 1000 Bq/dry kg until at least September 2012 [1]. This disproportional distribution of
73 radioisotopes was also observed in marine fish by Wada et al. Wada reported that the
74 retention time of radiocesium appears to be remarkably longer in the larvae of demersal fish,
75 e.g., *Sebastes cheni*, than in surface fish, e.g., *Eugraulis japonica* [2]. Similar disproportional
76 distributions among radionuclides was also reported in a terrestrial ecosystem. Nakanishi
77 et al. reported ^{110m}Ag accumulation in the orb-web spider (*Nephila clavata*) and other
78 arthropods [3]. Decay-corrected data from Nakanishi's work showed that the radioactivity
79 ratio between ^{110m}Ag and ^{137}Cs (^{110m}Ag/^{137}Cs) in specific samples of arthropods was over 1.0,
80 whereas the same ratio (^{110m}Ag/^{137}Cs) in the soil was 0.0014-0.0023, which indicates that

these organisms may actively accumulate radiosilver more than radiocesium. This finding is inconsistent with the majority of the organisms from land ecosystems, which accumulate more radiocesium than radiosilver.

These disproportional distributions may occur via partitioning in complex ecosystems and food webs through processes that include biological concentration. To better understand the fate of radioisotopes in nearshore marine environments, the present study sampled water, sediment, biofilms, macrobenthos and macroalgae as basic environmental materials and entry points of organic/inorganic materials into the ecosystem. In the present study, samples were collected using a self-contained underwater breathing apparatus (SCUBA) at a depth of 5-10 m along the nearshore area around Hisanohama Port. Sampling was essentially performed weekly from the end of November 2011 to the beginning of February 2012 at 6 different points. Our results showed that macroalgae and macrobenthos accumulate and retain both radiocesium and radiosilver. The observed ratios of radiosilver/radiocesium are variable among the organisms, and they may be dependent on the specific usage and behavior of the organisms with respect to metals, such as specific cofactors, oxygen acceptors, metal uptake and other metabolic features. Although sediment

97 also retains both radiocesium and radiosilver, biofilms contain only radiocesium. The
98 microbial community structure is likely related to the radiocesium accumulation and
99 retention in microbes.
100
101 Materials and Methods
102 Sampling
103 Sampling was performed from 11 November 2011 to 4 February 2012. The sampling site
104 was the ocean along the coastline of Hisanohama, Iwaki City, Fukushima, Japan. We
105 collected samples 10 times within the established time period at 11 Nov (week 1), 20 Nov
106 (week 2), 26 Nov (week 3), 3 Dec (week 4), 10 Dec (week 5), 17 Dec (week 6), 14 Jan (week 7),
107 21 Jan (week 8), 29 Jan (week 9) and 4 Feb (week 10). Sampling was performed at 6
108 different areas near Hisanohama Port: Area 1 (37.153762N 141.006167E, weeks 1 and 5),
109 Area 2 (approximately 37.149863N 141.001017E, weeks 2, 8 and 9), Area 3 (approximately
110 37.146579N 141.002390E, week 4), Area 3' (approximately 37.147503N 141.008570E, week
111 10), Area 4 (approximately 37.133887N 141.002390E, weeks 3 and 7) and Area 4'
112 (approximately 37.142953N 141.003592E, week 6). These sampling sites are located 30 km

113 south of the Fukushima Nuclear Power Plant #1. Sampling was performed by diving with a
114 SCUBA unit. Divers sampled the bottom water and surface water (5 L) and collected bottom
115 stones to obtain biofilms and locally observed macrobenthos and macroalgae.
116 Sediment core samples were collected at Area 2 using a piston corer prototype. The "core
117 sampler" was composed of a 4.5 cm diameter/28 cm height cylinder and inscribed piston.
118 Core samples were collected during a separate dive in weeks 6 (core sample 1) and 7 (core
119 samples 2 – 4).
120 Samplings were performed with permission from Fukushima Prefecture and the fishery
121 association of Iwaki City.
122
123 Sample preparation
124 The seawater samples were immediately filtered with two 24-mm-wide 0.22 μm Durapore
125 filters (Millipore, MA, USA) sample until they clogged. All samples were frozen at -20°C in a
126 field freezer prior to transportation back to laboratory.
127 In the laboratory, the samples were dried at 105°C overnight except for the filters, water
128 and sediment core samples. The dried samples were crushed by a food mill and settled into a

129 U8 container, and the weight and height were measured in the container. In the case of
130 biofilms, half of the samples was dried as mentioned above and the other half was captured
131 on 0.2 μm pore size membrane filters and stored at -20°C for ribosomal RNA gene analysis.
132 The water samples were dried by boiling. The remaining salts were settled into a U8
133 container, and the weight and height were measured in the container.
134 Sediment core samples for radioactivity measurements were stored at -80°C. The cores were
135 sliced by a clean saw at 5 cm intervals from the surface side of the sediment to the bottom
136 side. Each piece of the core sample was freeze dried and then settled into a U8 container,
137 and the weight and height measured in the container.
138
139 Measurement of radioactivity
140 The gamma ray activity of the samples in the containers was measured by a Germanium
141 (Ge) detector. The detector setup is identical to those described in [4]. The energy resolution
142 of 2 keV full width at half maximum (FWHM) was achieved at 1332.5 keV gamma rays. The
143 sample location and the detector were surrounded with 15 cm lead blocks to reduce the
144 background radiation in the gamma ray spectroscopy. The detection efficiency of the gamma

rays was calibrated with an accuracy of 2 - 10% using a multiple gamma ray standard source, which ranged from 88 keV to 1836 keV. A calibrated ^{134g}Cs source was also used to correct for the coincidence summing for radioactivity determinations of ^{134g}Cs.

Every sample was contained in a U8 plastic container. The U8 container is a standard container in Japan that is used for measurements of absolute radioactivity with high accuracy by a Ge detector. The geometry of the container is cylindrical, with a diameter of 47 mm and height of 60 mm. The volume is approximately 100 mL. The efficiency calibration source is available within the container with a uniform density in the container.

Every sample was measured by the Ge detector for at least 8 hours to obtain sufficient statistics for each gamma ray peak. The relative geometry between the sample and the Ge detector was carefully reproduced by a guide apparatus at the sample location.

Gamma rays from ^{134,137}Cs and ^{110m}Ag were observed for the majority of the samples. The radioactivity levels for every isotope were determined from the yield of the gamma rays corrected by the detection efficiency of the Ge detector and a geometrical acceptance between the sample and the detector. The geometry difference in the height of the sample from the calibration source was simulated by several electromagnetic simulation codes,

including Geant4 [5,6] and EGS5 [7].

The radioactivity of the marine animals, macroalgae and biofilm samples were normalized by weight, and the radioactivity of the water samples and sediment core samples were normalized by volume.

Element analysis

To quantitatively analyze the content of 37 elements (^{7}Li, ^{9}Be, ^{23}Na, ^{24}Mg, ^{27}Al, ^{39}K, ^{43}Ca, ^{45}Sc, ^{47}Ti, ^{51}V, ^{52}Cr, ^{55}Mn, ^{57}Fe, ^{59}Co, ^{60}Ni, ^{63}Cu, ^{66}Zn, ^{85}Rb, ^{88}Sr, ^{98}Mo, ^{111}Cd, ^{133}Cs, ^{139}La, ^{140}Ce, ^{141}Pr, ^{146}Nd, ^{152}Sm, ^{153}Eu, ^{158}Gd, ^{159}Tb, ^{164}Dy, ^{165}Ho, ^{166}Er, ^{169}Tm, ^{172}Yb, ^{175}Lu, and ^{202}Hg) in the samples (i.e., surface salts, surface microbes, biofilms), the samples were predigested with 5 mL of concentrated HNO_3 for 1 h at room temperature. Next, the organic components were completely decomposed by wet-ashing using a microwave sample preparation system (Multi-Wave-3000, Perkin Elmer, MA USA) [8]. The digested samples were brought up to a volume of 50 mL with MilliQ water (MQW) and filtered through 5B filter paper (Advantec, Tokyo, Japan). The concentrations of the mineral elements were determined by Inductively Coupled Plasma Mass Spectrometry (ICP-MS, NexION300, Perkin Elmer). For the ICP-MS

177 analysis, a portion of the filtrated samples was diluted appropriately with 0.01 mol L-1 HCl
178 [8]. The mineral nutrient concentration in the samples was calculated as a unit (mg g^{-1} in
179 dry weight).
180 The obtained ICP-MS data were normalized by the root-sum-of-squares (RSS) levels among
181 each element. Count data of radioactive cesium (^{134}Cs and ^{137}Cs) were treated with the same
182 calculation for normalization and then merged with the normalized ICP-MS dataset
183 (elements table).
184
185 ssrDNA analysis
186 Genomic DNA was prepared from stored biofilm samples by bead-beating with a
187 phenol:chloroform:isoamyl alcohol (PCI) extraction. Bead-beating was performed at 3000
188 rpm for 5 min (TOMY, Tokyo Japan), and then nucleic acids were recovered by ethanol
189 precipitation.
190 PCR amplification was performed with the extracted genomic DNA with two primer sets for
191 16S ssrDNA, 515F/806R [9,10], and 18S ssrDNA, TAReuk454FWD1/TAReukREV3 [11]. The
192 primers were modified for Illumina sequencing with a multi-index kit for the Nextera XT

193 sequencing library construction kit (Illumina, CA, USA). We added a "read1" sequence (5'-

194 TCG TCG GCA GCG TCA GAT GTG TAT AAG AGA CAG -3') to the forward primers and a

195 "read1" sequence (5'- GTC TCG TGG GCT CGG AGA TGT GTA TAA GAG ACA G -3') to the

196 reverse primers.

197 PCR was performed with a standard reaction of ExTaq DNA polymerase according to the

198 manufacturer's instructions (Takara Bio, Kyoto Japan) with 25 pmol of each primer/50 μl

199 reaction. The reactions were performed as a two-step PCR (10 cycles of 94°C for 30 s, 55°C

200 for 45 s and 72°C for 60 s followed by 20 cycles of 94°C for 30 s and 72°C for 60 s) for 16S and

201 3-step PCR (30 cycles of 94°C for 30 s, 55°C for 45 s and 72°C for 60 s) for 18S. The amplified

202 products were purified by 1% agarose gel electrophoresis. The obtained amplified products

203 were applied to the NexteraXT (Illumina CA USA) sequencing library construction process

204 without the "tagmentation" process.

205 A multi-index sequencing library was applied to the MiSeq sequencing kit v1 and read by

206 Illumina MiSeq according to the instructions in the paired-end sequencing mode. Data were

207 treated by MiSeq reporter software, and the reads were obtained from individual samples.

208 After the extraction of reads, reads from weeks 4, 5 and 8 for the 18S ssrDNA were

209 insufficient for analysis. Therefore, the following analysis was performed using reads from
210 weeks 1, 2, 3, 6, 7, 9 and 10.
211 The obtained read data were mapped onto the ribosomal RNA sequence library SILVA
212 release 108 by the program package QIIME [12] using “Prefix-suffix OTU picking”, and the
213 absolute abundance OTU table at the family level was constructed. Count zero data were
214 manually removed from the table, and the relative abundance values were calculated. 16S
215 data and 18S data were treated independently and then merged into a single OTU table
216 with the relative abundance values.
217 Sequence data have been deposited in the DDBJ sequence read archive with accession
218 number DRA004367.
219
220 Statistical analysis
221 For the statistical analysis, we used the program package R [13]. First, we drew a heatmap
222 chart with the hierarchical cluster analysis (HCA). The heatmap.3 function in the GMD
223 package, which is a package for non-parametric distance measurements between two
224 discrete frequency distributions [14], was used to draw the heatmap with the HCA.

225 Independent heatmaps were drawn from each element table and the OTU table with a
226 two-axis HCA. A scaling option was used for the OTU table treatment according to the row
227 direction but was not used for the elements table treatment.
228 A principal components analysis (PCA) was performed with the merged dataset, including
229 both the out table and elements table, using the prcomp function in R. Score plots were
230 drawn with principal component 1 (PC1) (x-axis) and PC2 (y-axis). The loading plots for
231 quadrants II and III were manually drawn.
232 Spearman's rank correlation coefficient between the elements dataset and the OTUs dataset
233 was calculated with the cor function in R. A correlation matrix was used to draw the
234 heatmap chart with the HCA using the heatmap.3 function of R.
235
236 Results and Discussion
237 Heterogeneous distribution of artificial radioisotopes in the coastal marine environment
238 around Hisanohama
239 According to our gamma ray energy spectra, we found significant peaks corresponding to
240 ^{134}Cs and ^{137}Cs in addition to natural radioisotope signals, such as ^{40}K (data not shown), for

241 all samples with the exception of the seawater samples. We also detected significant ^{110m}Ag
242 signals from the macrobenthos, macroalgae and sediment samples. Significant signals of the
243 radioisotopes ^{134}Cs, ^{137}Cs and ^{110m}Ag were not detected from the control samples taken from
244 Nishi-kawana inside Tokyo Bay, which is approximately 280 kilometers from the FDNPP.
245 Although ^{134}Cs (half-life of 2.0652 years) and ^{137}Cs (half-life of 30.1 years) from prior nuclear
246 weapons tests in the Pacific Ocean and the Chernobyl disaster might have persisted in the
247 seabed around Japan, our analysis of samples collected near Nishi-kawana did not detect
248 these signals. Therefore, we concluded that the radioisotopes detected in the samples in this
249 study originated from the FDNPP disaster rather than the environmental background or
250 past nuclear weapon tests.
251
252 As presented in Table 1, among the results from the radioactivity measurements of a variety
253 of samples, we noticed a heterogeneous distribution between radiocesium (^{134}Cs and ^{137}Cs)
254 and radiosilver (^{110m}Ag). The retention of radiocesium was observed in all sediments,
255 macrobenthos, macroalgae and biofilm samples, whereas non-detectable signals of these
256 isotopes were observed in the surficial and bottom water. This result is surprising because

257 the ^{134}Cs radioactivity detected in the Pacific Ocean near the accident site was 3900 Bq/m^3

258 (3.9 Bq/liter) in June 2011, which is one of the highest levels ever recorded [15]. Although

259 our results do not directly indicate that marine organisms and sediments are able to

260 accumulate radioisotopes at the concentrations found in this environment, we must consider

261 that they are able to retain radioisotopes for at least up to 9 months, which represents the

262 time lapse between the disaster and sample collection.

263

264 Table 1. Peak detection in the samples

	Peak detection		
Material	^{134}Cs	^{137}Cs	^{110m}Ag
Surface water	−	−	−
Bottom water	−	−	−
Particles in surface water *	−	−	−
Particles in bottom water *	−	−	−
Sediments	++	++	++
Macrobenthos	++	++	+

Macroalgae	++	++	+
Biofilms on bottom rocks	++	++	−

265 ++: significant peak detected from all samples

266 +: significant peak detected from certain samples (not all samples)

267 -: significant peak not detected from any sample

268 *: Particles were filtered from water using a 0.22 μm filter, and the radioactivity was

269 measured

270

271 Sediment core samples were obtained from the sampling point “Area 2” by the core sampler.

272 The analysis of these sediment core samples indicated the presence of both radiocesium and

273 radiosilver. The measured radioactivities are shown in Additional file 1: Supplementary

274 Table 1. To better understand the radioactivity in the same volume of space, we employ the

275 unit Bq/liter to express the radioactivity of the core samples because the core samples

276 contain different materials along their depth profile.

277 In Figure 1, the distribution of radioactivity along the sediment column is shown. Both

278 radiocesium and radiosilver are distributed similarly in the surficial part of the core

279 samples, which contains a large amount of radioactivity. The calculated regression line for
280 the data showed that both radiocesium and radiosilver occur at depths above approximately
281 155 mm. The similar distribution of radiocesium and radiosilver suggest that both
282 radioisotopes start to precipitate at almost the same time and they share a similar
283 precipitation pattern. The ratio of radioactivity between ^{110m}Ag and ^{137}Cs is 0.0046 on
284 average, which is based on the detected radiosilver of each 5 cm slice of the core samples
285 (Fig. 1b).
286
287 Figure 1
288 Radioactivity of the sliced sediment core. Panel a shows the results of ^{134}Cs, ^{137}Cs and ^{110m}Ag
289 measurements. Open circles indicate each sliced core sample. All 4 core samples were
290 collected inside Hisanohama Port (Area 2). Radioactivity is expressed as Bq/liter material.
291 The regression lines are calculated as linear approximation lines, and the R^2 value is
292 indicated beside each line. Panel b shows the ^{110m}Ag/^{137}Cs ratios. Panel a shows the
293 individual ^{110m}Ag/^{137}Cs ratio of each core slice.
294

295 In the macrobenthos and macroalgae samples, we also detected radiosilver and radiocesium.

296 However, the ratio between ^{110m}Ag and ^{137}Cs varied among the samples.

297 As shown in Figure 2a and Additional file 2: Supplementary Table 2, macroalgae contained

298 a relatively low ratio of radiosilver relative to radiocesium. The ratio between ^{110m}Ag and

299 ^{137}Cs averaged 0.06 to 0.07 among brown, red and calcareous algae (Fig. 2a); nevertheless, it

300 varied among individuals (Fig. 2b). Except for green algae, the ratio of ^{110m}Ag/^{137}Cs of

301 macroalgae was approximately 10-fold larger than that of the surrounding sediments. Green

302 algae contained almost no ^{110m}Ag.

303

304 Figure 2

305 Radioactivity of ^{134}Cs, ^{137}Cs and ^{110m}Ag in the macroalgae samples. Panel a shows the

306 average ^{110m}Ag/^{137}Cs ratio in the macroalgae sample, and panel b shows the individual

307 results for the macroalgae. The measured radioactivity is expressed by the bar graph.

308 Closed bars show ^{134}Cs, open bars show ^{137}Cs and gray bars show ^{110m}Ag. Radioactivity is

309 expressed as Bq/kg of dried sample (Bq/kg dry biomass).

310

311 Figure 3

312 Radioactivity of ^{134}Cs, ^{137}Cs and ^{110m}Ag in the macrobenthos samples. Panel a shows the

313 average ^{110m}Ag/^{137}Cs ratio in the macrobenthos sample, and panel b shows the individual

314 results for the macrobenthos. The measured radioactivity is expressed by the bar graph.

315 Closed bars represent ^{134}Cs, open bars represent ^{137}Cs and gray bars represent ^{110m}Ag.

316 Radioactivity is expressed as Bq/kg of the dry weight of the samples (Bq/kg dry biomass).

317 The arrowhead indicates the relatively high concentration of radiosilver found in the sponge

318 samples (i.e., the main body).

319

320 As shown in Figures 3a and 3b and Additional file 3: Supplementary Table 3, the

321 macrobenthos samples showed a variable ratio between ^{110m}Ag and ^{137}Cs.

322 Our results indicated that sea snails (Buccinidae) and oysters (*Crassostrea gigas*)

323 consistently presented a high ratio of ^{110m}Ag/^{134}Cs, which was also observed for the sponge

324 *Cliona chilensis*. Samples of the Ascidian *Halocynthia roretzi* showed a relatively high ratio

325 of ^{110m}Ag/^{134}Cs (Fig. 3a).

326 Certain mollusks, such as sea snails and oysters, are known to use hemocyanin as an oxygen

327 carrier [16]. A study on the relatively high ratio of ^{110m}Ag/^{137}Cs in the spider, *Atypus karschi*
328 indicated that the reaction center Cu in hemocyanin can be replaced by Ag, or ^{110m}Ag in this
329 case [3]. Similarly, the sampled mollusks may have actively incorporated ^{110m}Ag from
330 environmental water and taken up the radioisotope into the blood system. To corroborate
331 this hypothesis, our results showed a higher ratio of radiosilver compared with that of
332 radiocesium detected in the body (^{134}Cs = 21.7923, ^{137}Cs = 37.3885, ^{110m}Ag = 134.6388 (Bq/kg
333 dry biomass)) than in the shell (^{134}Cs = 12.6245, ^{137}Cs = 18.8071, ^{110m}Ag = 17.7947 (Bq/kg dry
334 biomass)).
335 A similar mechanism for accumulation and retention of the relatively high observed amount
336 of radiosilver in *Halocynthia roretzi* is expected. Ascidians accumulate vanadium into their
337 blood cells [17]. Although the function of vanadium accumulation is not yet fully understood
338 and the mechanism of metal uptake in ascidians is still under investigation, these
339 organisms may accumulate other metals using vanadium binding protein(s). Our samples of
340 ascidians are from *Halocynthia roretzi,* and a high specificity for vanadium has not been
341 reported in this species [18]. Our hypothesis is that a metal binding factor within the
342 *Halocynthia roretzi* blood system with a low specificity for vanadium is able to promote

343 ^{110m}Ag accumulation. Although our hypothesis is based on indirect evidence, it is partially
344 supported by the observation that the *Halocynthia roretzi* body (including the blood system)
345 showed a larger amount of radiosilver than was found in the shell, which can contain
346 radiosilver because of attached organisms on the surface of the shell. We investigated three
347 individuals of *Halocynthia roretzi*, and the body measurement results are ^{134}Cs = 645,0563,
348 927.5638, 944.2312; ^{137}Cs = 997.5926, 1437.1948, 1588.1469; ^{110m}Ag = 295.6794, 255.9421,
349 213.5846 (Bq/kg dry biomass) and the shell measurement results are ^{134}Cs = 18.6579,
350 51.1889, 28.2958; ^{137}Cs = 30.3881, 80.5451, 43.8699; ^{110m}Ag = not detected, 3.3797, not
351 detected (Bq/kg dry biomass).
352 The sea urchin (*Anthocidaris crassispina*) samples and the majority of the sponge samples
353 (*Cliona chilensis*) presented ratios of radiosilver/radiocesium that were lower relative to that
354 of the other macrobenthos (Fig. 3a, b). Nevertheless, the feeding pattern of sea urchins and
355 sea snails are similar because they are both deposit feeders, and the feeding patterns of
356 sponges, oysters and Ascidians are also similar because they are all filter feeders.
357 Interestingly, 4 of the 16 specimens of sponge presented remarkably high
358 radiosilver/radiocesium ratios of approximately 0.5 (Fig. 3b, arrowheads). Variation were

359 not observed in the radiosilver/radiocesium ratio corresponding to the three color variations
360 of the samples of *Cliona chilensis*. A previous report showed that certain sponge species
361 exhibit a strong ability to incorporate a variety of metal elements, including silver [19].
362 Indeed, sponges are known as "a sentinel organism" that can be used as a marker to monitor
363 heavy metal pollution in water because they present a high capacity for specific metal
364 accumulation [20]. According to Genta-Jouve et al., *Acanthella acuta*, which is a species of
365 commonly found sponge, can incorporate ^{110m}Ag from the surrounding water and retain the
366 element even after moving to clean water that does not contain ^{110m}Ag [19]; however, among
367 the six sponge species analyzed in that study, this feature was only observed in *Acanthella*
368 *acuta*. In our study, four specimens of sponge incorporated relatively high ratios of
369 radiosilver relative to radiocesium (Fig. 3b arrowhead); therefore, we regarded these
370 sponges as a "silver accumulator" species.
371 Thus, macroalgae and macrobenthic species present varying capacities to incorporate and
372 retain radioisotopes based on their biological features. In addition, the
373 radiosilver/radiocesium ratios of these organisms are higher than those in the sediment.
374 Although we detected both radiocesium and radiosilver from almost all biological samples in

375 this research, an interesting exception was observed because radiosilver was not detected in
376 any of the biofilm samples, including biofilms collected from Area 2 (weeks 2, 8 and 9) (Table
377 2). This result suggested that microbes that compose biofilms specifically accumulate and
378 retain radiocesium but not radiosilver, even when the surface of nearby sediments contains
379 both radioisotopes.
380
381 Table 2. Radioactivity of the biofilm samples

		^{134}Cs Bq/kg dry	^{137}Cs Bq/kg dry	^{110m}Ag Bq/kg dry
Week1	Area1	1141.77	1655.17	nd
Week2	Area2	671.00	932.18	nd
Week3	Area4	306.90	429.21	nd
Week4	Area3	429.21	2353.58	nd
Week5	Area1	926.40	1436.73	nd
Week6	Area4'	538.56	829.08	nd
Week7	Area4	844.49	1543.05	nd
Week8	Area2	818.66	1607.65	nd

Week9	Area2	359.77	591.46	nd
Week10	Area3'	190.29	294.20	nd

382 nd: not detected

383

384 "Cesium-philic" biofilm

385 Microbial communities that grow on surfaces of solid materials in the presence of water are

386 known as biofilms. Our observations suggest that the biofilm community specifically

387 accumulates radiocesium. Therefore, we analyzed the relationship between the microbial

388 consortia within the biofilms and their elemental composition.

389 Quantified element data were combined with radioactivity data for radiocesium and utilized

390 for the statistical analysis. Ribosomal RNA genes were sequenced and used to construct a

391 dataset for the statistical analysis.

392 A HCA from the dataset of elements and radiocesium (Fig. 4) in which an accumulation of

393 radioactive cesium, Cr, Ni, Sc, Rb, Li and cesium (Cs cluster) was performed for the week 1

394 sample. Another remarkable profile from the elemental analysis is observed in week 3,

395 where high relative amounts of lanthanide elements were measured (Lanth cluster).

Figure 4

Heatmap chart of the element and radioactivity data from the biofilm samples based on the hierarchical clustering analysis (HCA). The heatmap chart was sorted by the HCA for both axes (elements axis and sample axis). Boxes indicate clusters of radiocesium (Cs cluster) or lanthanides (Lanth cluster).

A PCA score plot (Fig. 5a) of the merged dataset between the elements/radiocesium and the microbial consortia showed that the week 1 sample was placed in the PC1 negative – PC2 positive direction and the week 3 sample was placed in the PC1 negative – PC2 negative direction. As mentioned above, the week 1 sample contained high relative amounts of the Cs cluster signals, and the week 3 sample contained high relative amounts of the Lanth cluster signals. Consistent with those findings, the PCA loading plot showed that the Cs cluster was placed in the PC1 negative – PC2 positive direction (Fig. 5b, Additional file 4: Supplementary Table 4), and the lanthanide cluster was placed in the PC1 negative – PC2 negative direction (Fig. 5b, Additional file 5: Supplementary Table 5). The results of the

412 HCA and PCA analyses suggested that a “cesium-philic” biofilm occurred at the sampling

413 point in week 1 and a “lanthanide-philic” biofilm occurred at the sampling point in week 3.

414

415 Figure 5

416 PCA results among the sampling sites with microbial consortia data and element data with

417 radiocesium. Panel a is the score plot of the PCA among sampling sites. Each colored dot

418 indicates each sampling site. The color code is superimposed on the PCA score plot. Panel b

419 indicates the loading plot of the elements data. The upper panel shows the plot of elements

420 that contribute to the PC1 minus and PC2 plus direction, indicating that they contribute to

421 separate week 1 samples in the PC1 minus and PC2 plus direction. The lower panel shows

422 the plot of elements that contribute to the PC1 minus and PC2 minus direction, indicating

423 that they contribute to separate week 3 samples in the PC1 minus and PC2 minus direction

424 in the PCA score plot. Panel c indicates the loading plot of the microbial consortia data. The

425 upper panel displays the plot of OTUs that contribute to the PC1 minus and PC2 plus

426 direction, indicating that they contributes to separate week 1 samples in the PCA score plot.

427 The lower panel shows the plot of the OTUs that contribute to the PC1 minus and PC2

428 minus direction, indicating that they contribute to separate week 3 samples in the PCA

429 score plot.

430

431 The PCA results from both datasets of elements and microbes showed candidate microbes in

432 the “cesium-philic” and “lanthanide-philic” biofilms on the loading plots because those plots

433 were placed in same loading direction, e.g., PC1 negative – PC2 positive (Cs cluster) or PC1

434 negative – PC2 negative (Lanth cluster) (Fig. 5c, Additional file 4 and 5: Supplementary

435 Table 4 and 5). Indeed, the HCA heat map of the microbial consortia showed that the PC1

436 negative – PC2 negative-directed microbes mainly appeared in the week 1 column (Fig. 6

437 blue dots). The same tendency was observed with the Lanth cluster microbes (Fig. 6 green

438 dots). These results suggest that these two OTU sets are positively correlated with the

439 Lanth cluster (week 3 sample) and Cs cluster (week 1 sample). The correlation heat map

440 chart between the element dataset and the OTU dataset supports this result

441

442 Figure 6

443 Heatmap chart of microbial consortia data for biofilms with a hierarchical clustering

444 analysis (HCA).

445 The heatmap chart has been sorted by the HCA for both axes (OTU axis and sample axis).

446 Green and blue dots indicate contributing OTUs for the PC1 minus and PC2 plus direction

447 and the PC1/PC2 minus direction, respectively. The relative intensity value has been scaled

448 and centered in the row direction.

449

450 The radiocesium and Cs cluster elements are positively correlated to other multicellular

451 eukaryotes, such as *Hexacorallia* and *Oligochaete*. For bacteria, high relative intensities of

452 *Bacteroidetes*, *Rhodobacteraceae* and Gamma-proteobacteria were observed (Additoinal file

453 6: Supplementary Table 6 and Fig. 6). Although a primer set that did not target Archaea

454 was used, Archeal sequences were obtained in this work by sequencing amplicons generated

455 by the 16S ribosomal RNA primers set. An uncultured Crenarcheota in marine group I was

456 observed to be one of the dominant OTUs from the biofilm sample of week 1 (Additional file

457 6: Supplementary Table 6).

458 The function of these microorganisms is poorly understood. However, Alpha- and

459 Gamma-proteobacteria have been obtained from biofilms on the surface of nuclear fuel pools

[21]. According to Sarro et al. [21], biofilms obtained from nuclear fuel pools accumulate ^{60}Co. Cobalt accumulation in the week 1 sample was suggested by the PCA (Fig. 5b and Additional file 4: Supplementary Table 4) despite a lack of ^{60}Co signal indicated by gamma-ray spectrography. The microbial community retrieved from the nuclear fuel pool was described as capable of accumulating both ^{60}Co and ^{137}Cs as reported by Tisakova et al. [22]. Our results suggest that the biofilm sampled in week 1 presents similar characteristics to the microbes described by Sarro et al. and Tisakova et al.

Conclusions

In this study, we found heterogeneous distributions of radiocesium and radiosilver among a variety of sample types from the coastal environment near the FDNPP disaster. Specific organisms that use hemocyanin, such as shell fish and Ascidians, accumulate and retain ^{110m}Ag, and similar observations have been reported in terrestrial spiders. We also found radiosilver in the sediment samples, suggesting that particular materials can be sources of radiosilver for these organisms, even if particles filtered from the water have low levels of radioactivity in our samples.

476 However, the biofilm samples did not display detectable signals of radiosilver, although the
477 amount of radiocesium in these samples was higher than that found in other marine
478 organisms. Biofilms may still act as an entry point for radiocesium to enter into the
479 ecosystem. In this paper, we could not assess the functional mechanisms by which biofilms
480 accumulate cesium specifically; thus, future research that includes cultivation experiments
481 and meta-transcriptome analyses should be performed to further investigate the microbial
482 communities described in this work and provide insights into this complex topic.
483

484 Declarations

485 Author's contributions

486 SM, HO and JS designed research. SM, HO, KK, HY and JS performed sampling. YK and
487 MI performed ICP-MS analysis and KS and JK partially performed sample preparation for
488 ICP-MS and advice for statistical analysis. Sample preparation and molecular biological
489 experiment was performed by SM and KK. Radioactivity measurement has been done by
490 HO. SCUBA diving safety control and sampling arrangement has been done by HY and JS.
491

492 Acknowledgements

493 Sampling was permitted by the Iwaki City Fishery Association and performed via the

494 fishing vessel Shyo-ei-maru and crew, which belong to the abalone section of the Iwaki

495 Fishery Association. The diving safety of SM was overseen by Toshiyuki Suzuki. The

496 authors wish to acknowledge the profound academic comments and proofreading provided

497 by R. Craig Everroad and Diogo M. O. Ogawa.

498

499 Competing interests

500 The authors declare no competing financial interests.

501

502 Availability of data and materials

503 The datasets used and/or analysed during the current study except for ribosomal RNA

504 sequences data and datasets that showed in manuscript or supplementary tables are

505 available from the corresponding author on reasonable request.

506 Ribosomal RNA sataset are available in the DDBJ sequence read archive with accession

507 number DRA004367.

508 Electronic supplementary material

509

510 Additional file 1: Supplementary Table 1: Radio activity of core samples. (XLSX 44 KB)

511

512 Additional file 2: Supplementary Table 2: Radio activity of macro algae samples. (XLSX 47

513 KB)

514

515 Additional file 3: Supplementary Table 3: Radio activity of macro benthos samples. (XLSX

516 46 KB)

517

518 Additional file 4: Supplementary Table 4: Loading plot on PC1 minus - PC2 plus. (XLSX 52

519 KB)

520

521 Additional file 5: Supplementary Table 5: oading plot results of PC1 minus - PC2 minus.

522 (XLSX 51 KB)

523

524 Additional file 6: Supplementary Table 6: Cs cluster taxon in Week1 sample. (XLSX 30 KB)

525

526 Funding

527 This work was supported by RIKEN Incentive Research Project (FY2011) "Emergency
528 monitoring for possible cycling of radio active compounds via oceanic food web" (SM, HO)
529 and biofilm section was supported by MEXT Grant-in-Aid for Scientific Research on
530 Innovative Areas Grant Number 23117003 (SM, KK).

531

532 References

533 1. Kanda J. Long-term Sources: To what extent are marine sediments, coastal groundwater,
534 and rivers a source of ongoing contamina;on? The Accidents at Fukushima Dai-Ichi,
535 Exploring the Impacts of Radiation on the Ocean. Tokyo; 2012. pp. 1–19. Available from:
536 http://www.whoi.edu/fileserver.do?id=138584&pt=2&p=141569

537 2. Wada T, Nemoto Y, Shimamura S, Fujita T, Mizuno T, Sohtome T, et al. Effects of the
538 nuclear disaster on marine products in Fukushima. Journal of Environmental Radioactivity.
539 Elsevier Ltd; 2013;124:246–254.

3. Nakashima H, Mori A, Takeda K, Tanaka H, Kobayashi N, Tanoi K, et al. Discovery of radioactive silver (^{110m}Ag) in spiders and other fauna in the terrestrial environment after the meltdown of Fukushima Dai-ichi nuclear power plant. Proceedings of the Japan Academy. Ser. B: Physical and Biological Sciences. 2015;91:160–174.

4. Haba H, Kanaya J, Mukai H, Kambara T, Kase M. One-year monitoring of airborne radionuclides in Wako, Japan, after the Fukushima Dai-ichi nuclear power plant accident in 2011. Geochem. J. 2012;46:271–278.

5. Agostinelli S, Allison J, Amako K, Apostolakis J, Araujo H, Arce P, et al. Geant4—a simulation toolkit. Nuclear Instruments and Methods in Physics Research Section A: Accelerators, Spectrometers, Detectors and Associated Equipment. 2003;506:250–303.

6. Allison J, Amako K, Apostolakis J. IEEE Xplore Abstract - Geant4 developments and applications. Nuclear Science. 2006;53;270-278.

7. Hirayama H, Namito Y, Nelson WR, Bielajew AF, Wilderman SJ, Michigan U. The EGS5 code system. United States. Department of Energy. 2005;No. SLAC-R-730.

554 8. Itouga M, Kato Y, Sakakibara H. Phenotypic plasticity and mineral nutrient uptake of
555 the moss Polytrichum commune Hedw. (Polytrichaceae, Bryophyta) during acclimation to a
556 change in light intensity. Hikobia. 2014;16:459–466.

557 9. Caporaso JG, Lauber CL, Walters WA, Berg-Lyons D, Lozupone CA, Turnbaugh PJ, et al.
558 Global patterns of 16S rRNA diversity at a depth of millions of sequences per sample.
559 Proceedings of the National Academy of Sciences. 2011;108 Suppl 1:4516–4522.

560 10. Caporaso JG, Lauber CL, Walters WA, Berg-Lyons D, Huntley J, Fierer N, et al.
561 Ultra-high-throughput microbial community analysis on the Illumina HiSeq and MiSeq
562 platforms. ISME J. 2012;6:1621–1624.

563 11. Stoeck T, Bass D, Nebel M, Christen R, Jones MDM, Breiner H-W, et al. Multiple
564 marker parallel tag environmental DNA sequencing reveals a highly complex eukaryotic
565 community in marine anoxic water. Mol Ecol. 2010;19 Suppl 1:21–31.

566 12. Caporaso JG, Kuczynski J, Stombaugh J, Bittinger K, Bushman FD, Costello EK, et al.
567 QIIME allows analysis of high-throughput community sequencing data. Nat. Methods.
568 2010;7:335–336.

569 13. Team RC. R: A language and environment for statistical computing [Internet]. R
570 Foundation for Statistical Computing, editor. www.R-project.org. Vienna, Austria; 2014
571 [cited 2016 May 24]. Available from: http://www.R-project.org/

572 14. Zhao X, Valen E, Parker BJ, Sandelin A. Systematic clustering of transcription start site
573 landscapes. PLoS ONE. 2011;6:e23409.

574 15. Buesseler KO, Jayne SR, Fisher NS, Rypina II, Baumann H, Baumann Z, et al.
575 Fukushima-derived radionuclides in the ocean and biota off Japan. Proceedings of the
576 National Academy of Sciences. 2012;109:5984–5988.

577 16. van Holde KE, Miller KI, Lang WH. Molluscan Hemocyanins: Structure and Function.
578 Blood and tissue oxygen carriers. Berlin, Heidelberg: Springer Berlin Heidelberg; 1992. pp.
579 257–300.

580 17. Ueki T, Michibata H. Molecular mechanism of the transport and reduction pathway of
581 vanadium in ascidians. Coordination Chemistry Reviews. Elsevier B.V; 2011;255:2249–
582 2257.

583 18. Michibata H, Terada T, Anada N, Yamakawa K. The accumulation and distribution of

584 vanadium, iron, and manganese in some solitary ascidians. The Biological Bulletin.

585 1986;171;672-681.

586 19. Genta-Jouve GG, Cachet N, Oberhänsli F, Noyer C, Teyssié J-L, Thomas OP, et al.

587 Comparative bioaccumulation kinetics of trace elements in Mediterranean marine sponges.

588 Chemosphere. Elsevier Ltd; 2012;89:340–349.

589 20. Berthet B, Mouneyrac C, Pérez T, Amiard-Triquet C. Metallothionein concentration in

590 sponges (Spongia officinalis) as a biomarker of metal contamination. Comparative

591 Biochemistry and Physiology Part C: Toxicology & Pharmacology. 2005;141:306–313.

592 21. Sarró MI, García AM, Moreno DA. Biofilm formation in spent nuclear fuel pools and

593 bioremediation of radioactive water. Int. Microbiol. 2005;8:223–230.

594 22. Tišáková L, Pipíška M, Godány A, Horník M, Vidová B, Augustín J. Bioaccumulation of

595 137Cs and 60Co by bacteria isolated from spent nuclear fuel pools. J Radioanal Nucl Chem.

596 2012;295:737–748.

597

Fig.1

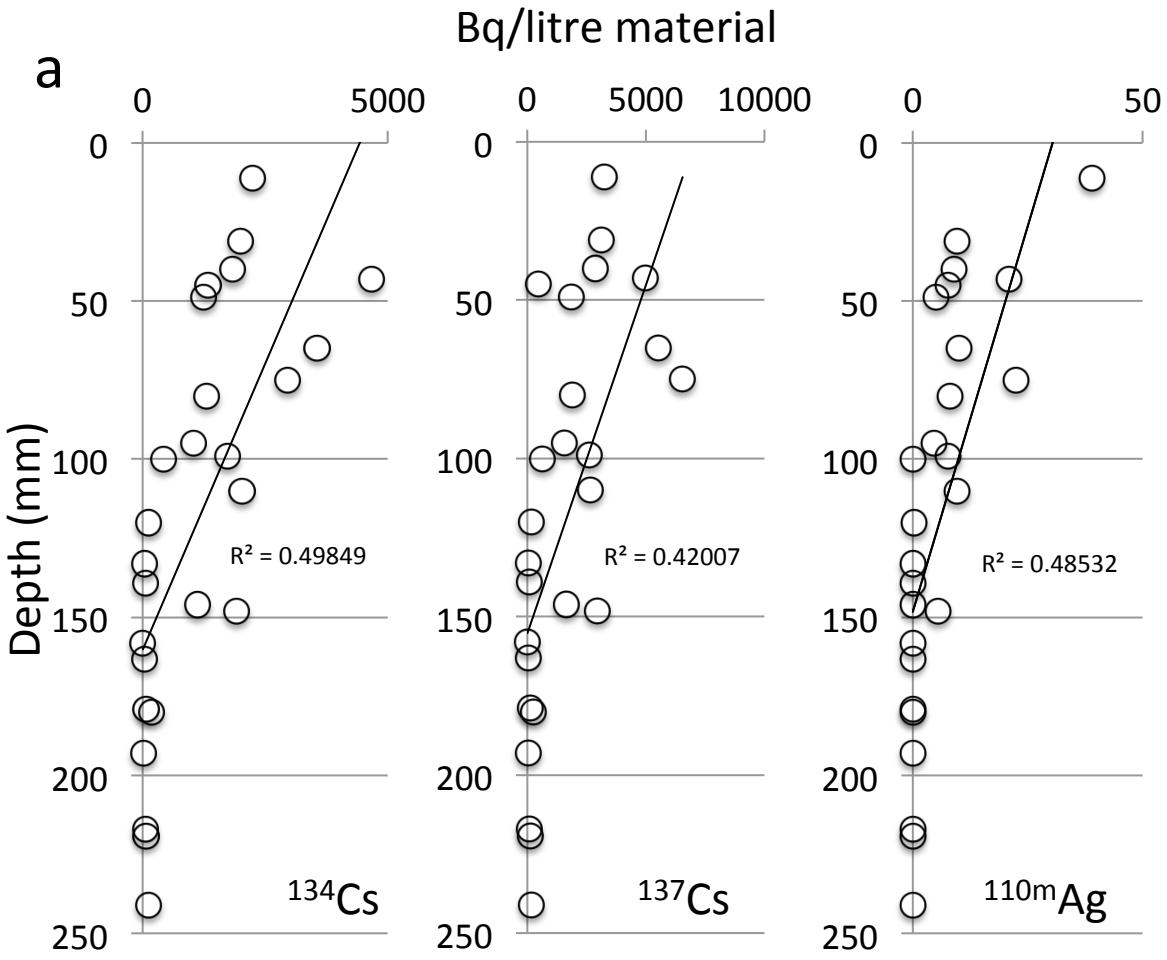
a
Bq/litre material
0
5000
0
5000
10000
0
50
Depth (mm)
0
50
100
150
200
250
R² = 0.49849
R² = 0.42007
R² = 0.48532
134Cs
137Cs
110mAg

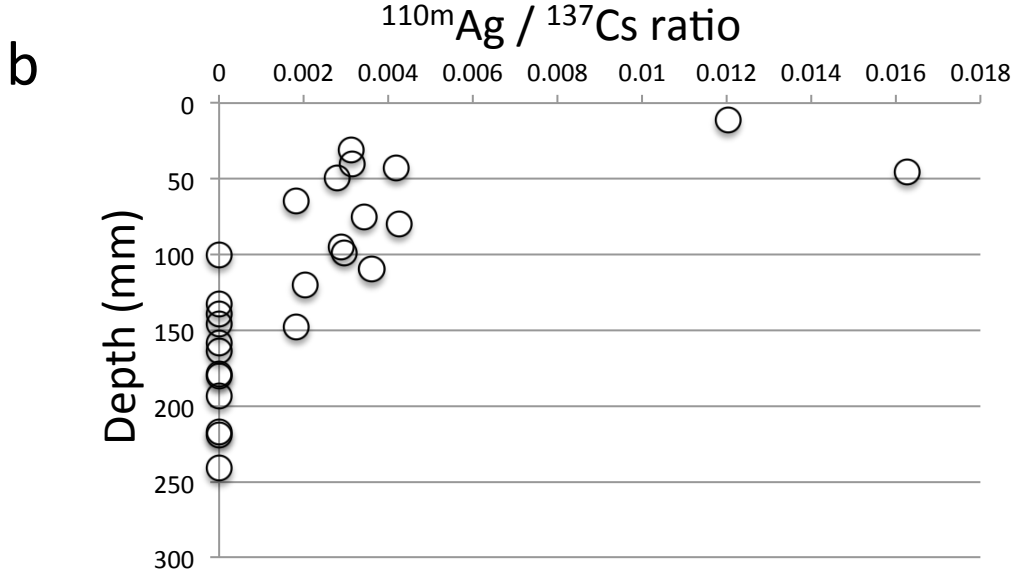
b
110mAg / 137Cs ratio
0
0.002
0.004
0.006
0.008
0.01
0.012
0.014
0.016
0.018
Depth (mm)
0
50
100
150
200
250
300

Fig.2

a

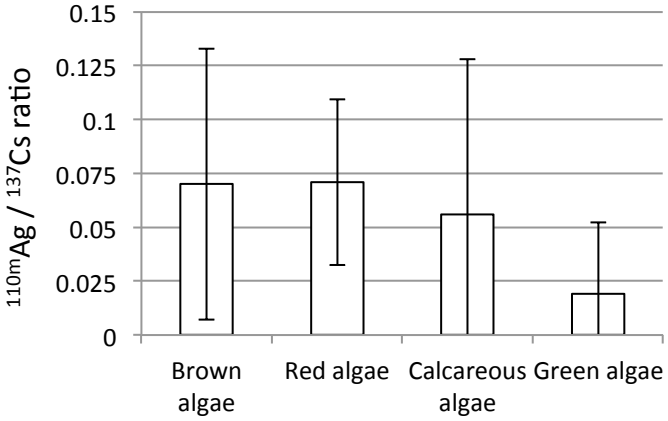
0.15
0.125
0.1
0.075
0.05
0.025
0
^{110m}Ag / ^{137}Cs ratio
Brown algae
Red algae
Calcareous algae
Green algae

b

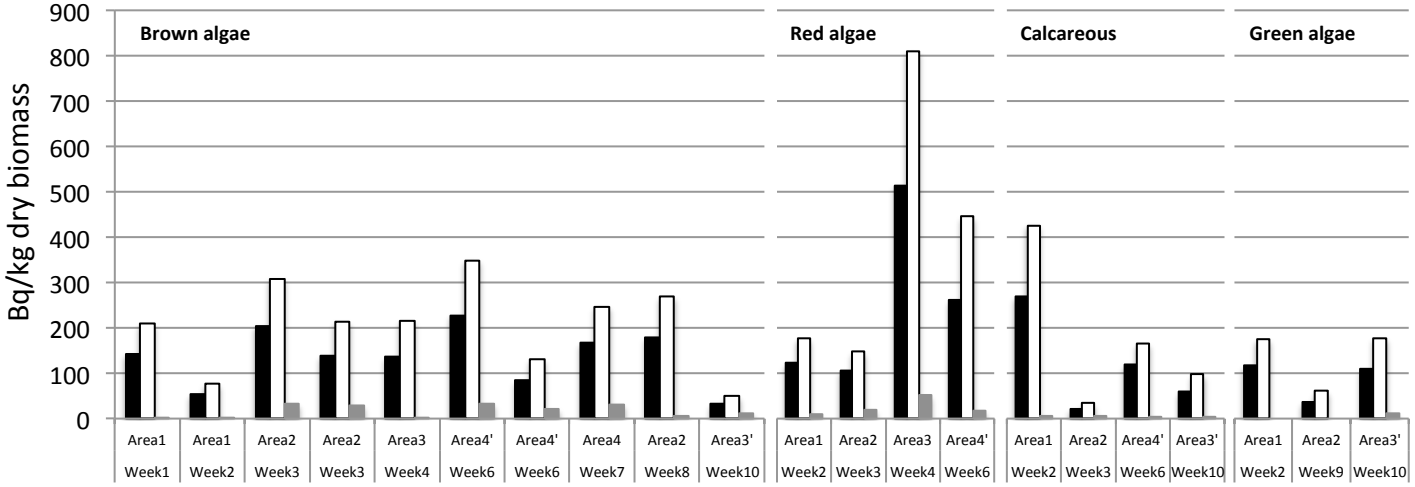
900
800
700
600
500
400
300
200
100
0
Bq/kg dry biomass
Brown algae
Red algae
Calcareous
Green algae
Area1 Week1
Area1 Week2
Area2 Week3
Area2 Week3
Area3 Week4
Area4' Week6
Area4' Week6
Area4 Week7
Area2 Week8
Area3' Week10
Area1 Week2
Area2 Week3
Area3 Week4
Area4' Week6
Area1 Week2
Area2 Week3
Area4' Week6
Area3' Week10
Area1 Week2
Area2 Week9
Area3' Week10

Fig.3

a

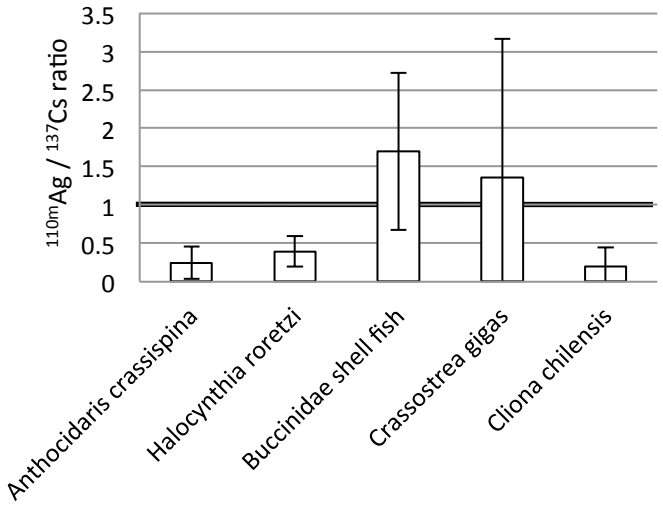
^{110m}Ag / ^{137}Cs ratio
3.5
3
2.5
2
1.5
1
0.5
0
Anthocidaris crassispina
Halocynthia roretzi
Buccinidae shell fish
Crassostrea gigas
Cliona chilensis

b

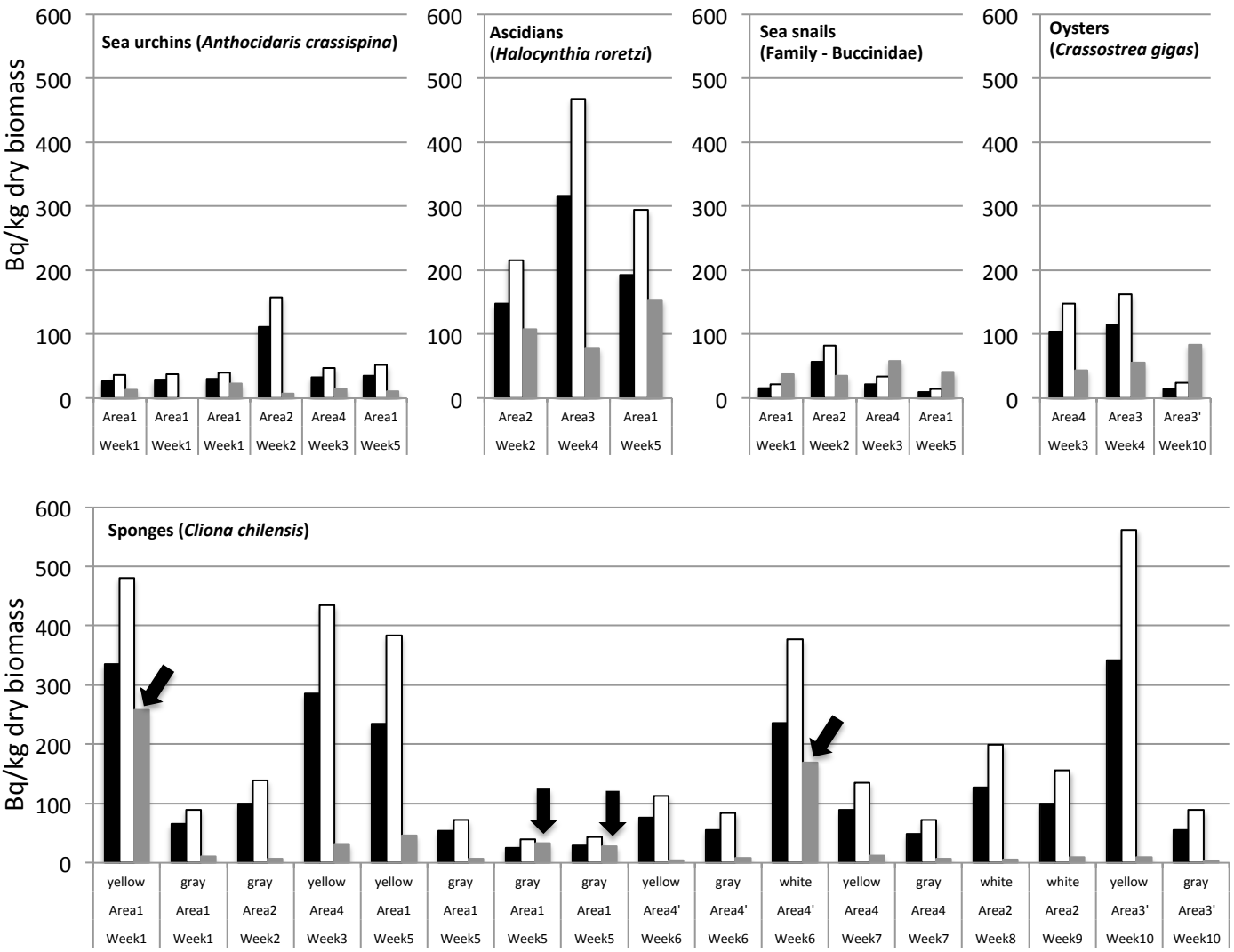
Bq/kg dry biomass
600
500
400
300
200
100
0
Sea urchins (*Anthocidaris crassispina*)
Area1 Week1
Area1 Week1
Area1 Week1
Area2 Week2
Area4 Week3
Area1 Week5
Ascidians (*Halocynthia roretzi*)
Area2 Week2
Area3 Week4
Area1 Week5
Sea snails (Family - Buccinidae)
Area1 Week1
Area2 Week2
Area4 Week3
Area1 Week5
Oysters (*Crassostrea gigas*)
Area4 Week3
Area3 Week4
Area3' Week10
Sponges (*Cliona chilensis*)
yellow Area1 Week1
gray Area1 Week1
gray Area2 Week2
yellow Area4 Week3
yellow Area1 Week5
gray Area1 Week5
gray Area1 Week5
gray Area1 Week5
yellow Area4' Week6
gray Area4' Week6
white Area4' Week6
yellow Area4 Week7
gray Area4 Week7
white Area2 Week8
white Area2 Week9
yellow Area3' Week10
gray Area3' Week10

Fig.4

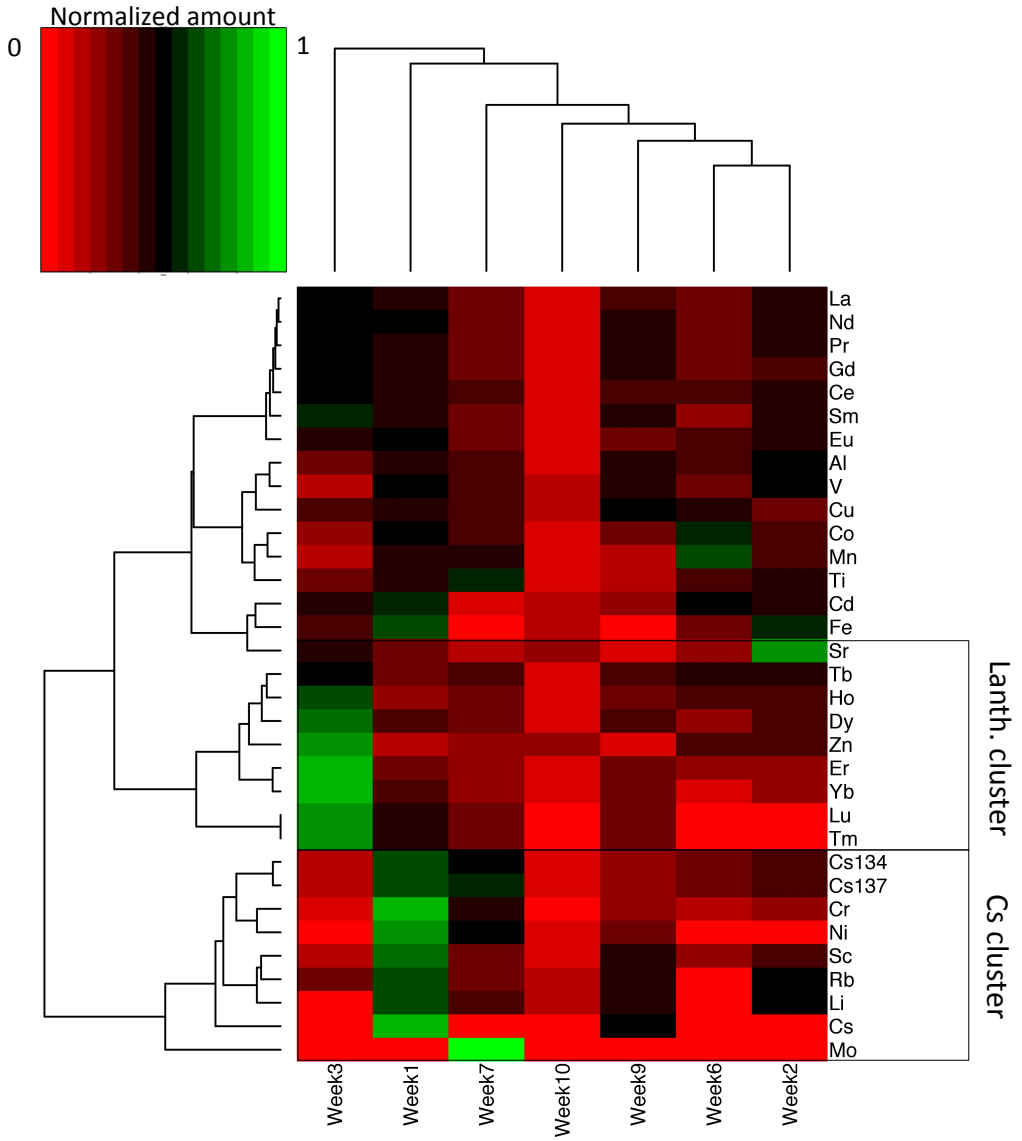
Normalized amount
0
1
La
Nd
Pr
Gd
Ce
Sm
Eu
Al
V
Cu
Co
Mn
Ti
Cd
Fe
Sr
Tb
Ho
Dy
Zn
Er
Yb
Lu
Tm
Cs134
Cs137
Cr
Ni
Sc
Rb
Li
Cs
Mo
Lanth. cluster
Cs cluster
Week3
Week1
Week7
Week10
Week9
Week6
Week2

Fig.5

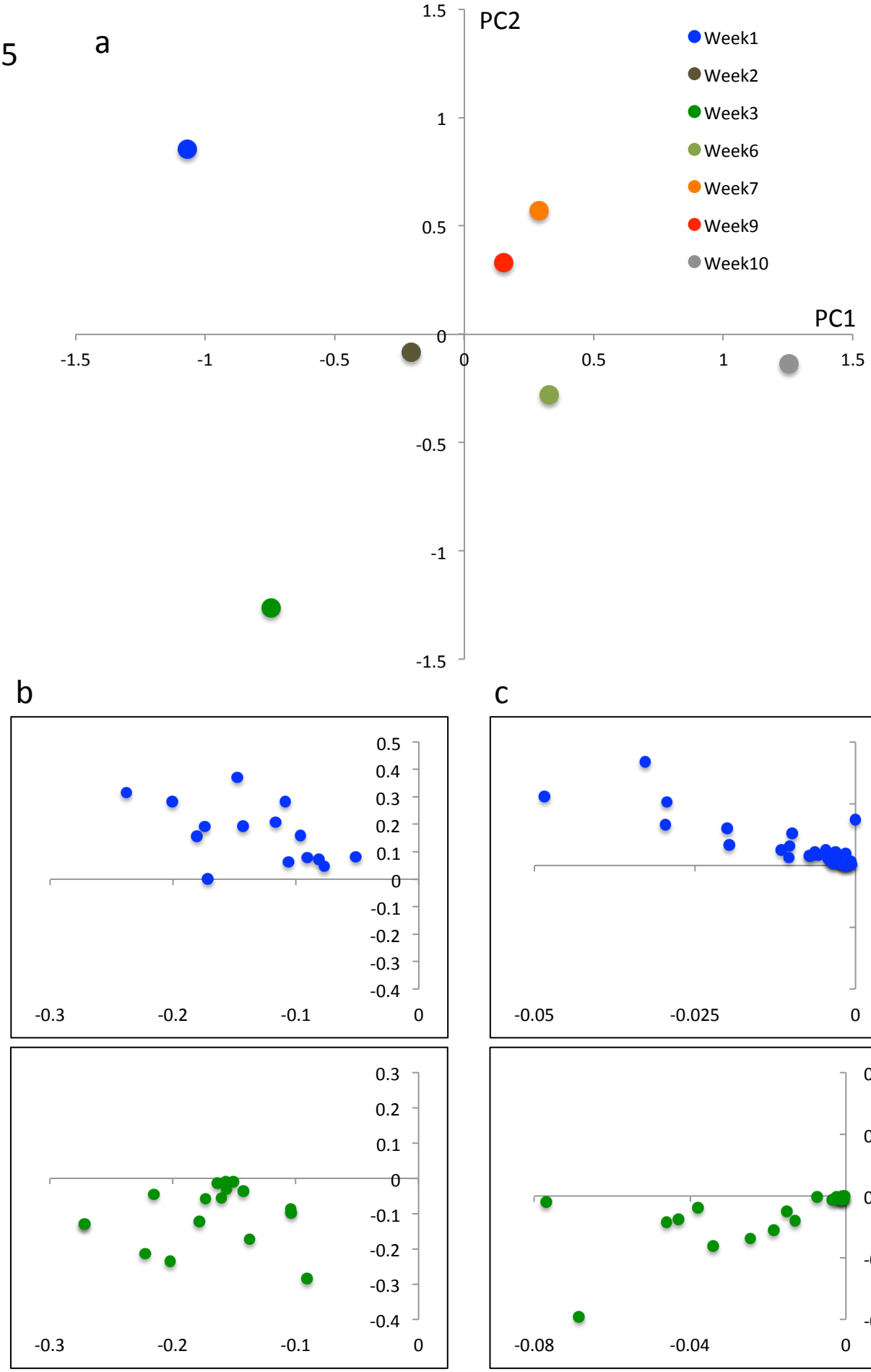
a
PC2
PC1
Week1
Week2
Week3
Week6
Week7
Week9
Week10
1.5
1
0.5
0
-0.5
-1
-1.5
b
c
0.5
0.4
0.3
0.2
0.1
0
-0.1
-0.2
-0.3
-0.4
-0.3
-0.2
-0.1
0
0.06
0.03
0
-0.03
-0.06
-0.05
-0.025
0.15
0.075
-0.075
-0.15
-0.08
-0.04

Fig.6

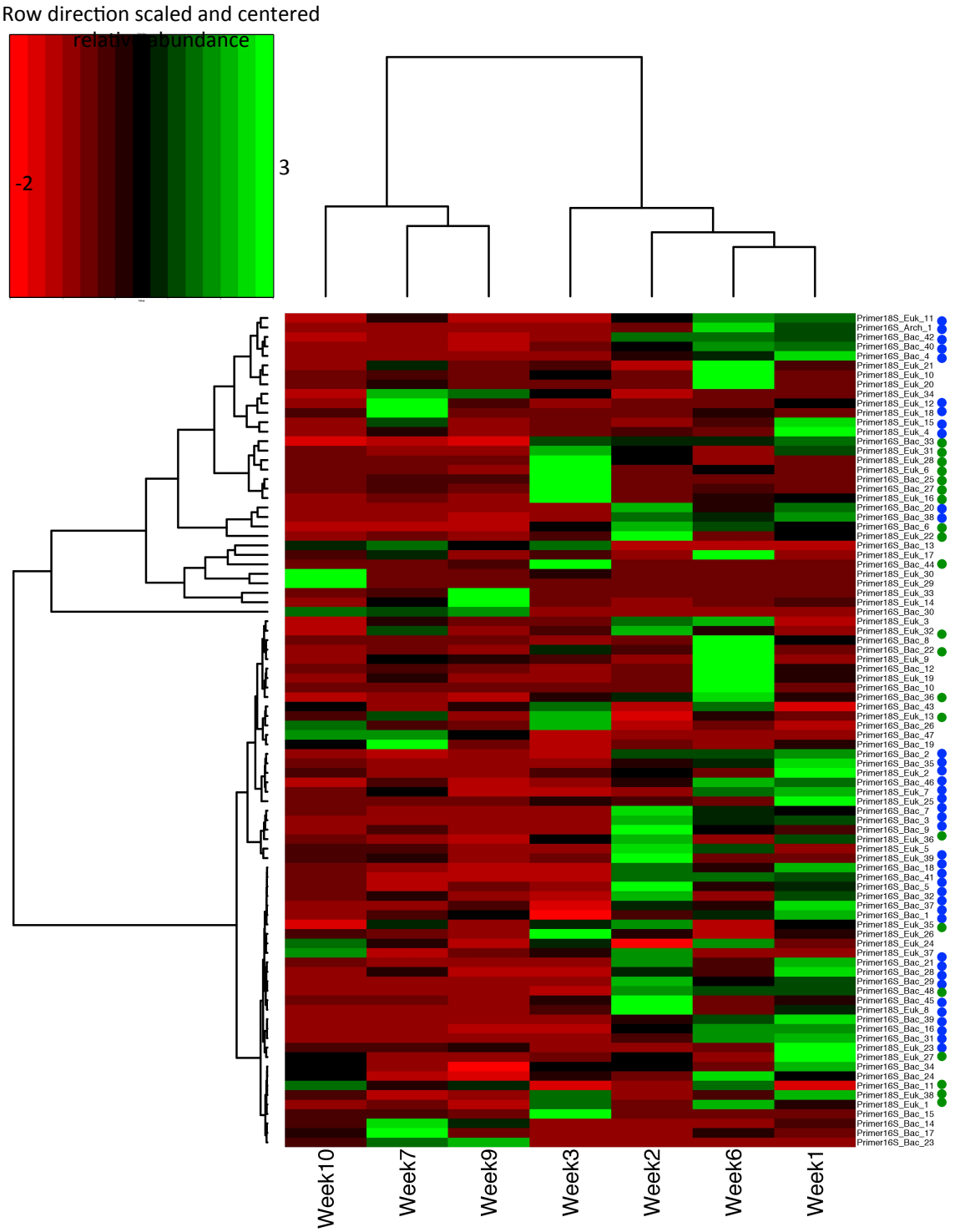
Row direction scaled and centered
relative abundance
-2
3
Week10
Week7
Week9
Week3
Week2
Week6
Week1